Observation of planar Hall effect in topological insulator—Bi$_2$Te$_3$

Archit Bhardwaj, Syam Prasad P., (iD) Karthik V. Raman, et al.

View Online   Export Citation   CrossMark

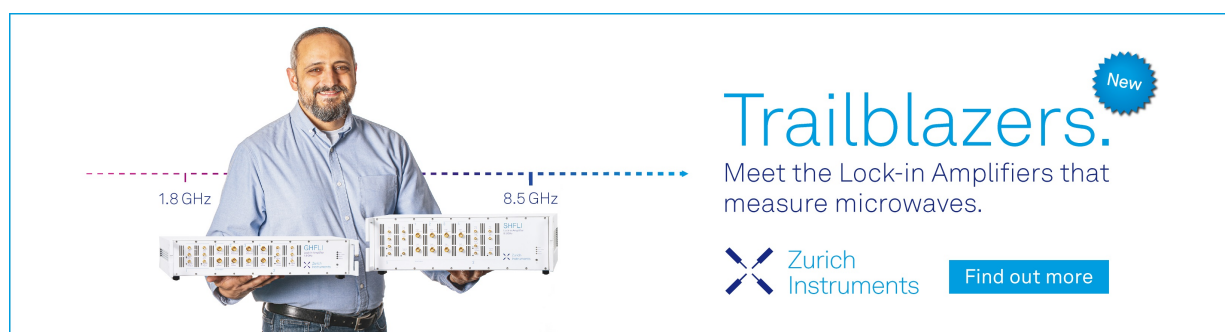## ARTICLES YOU MAY BE INTERESTED IN

Planar Hall effect in PtSe$_2$
Journal of Applied Physics **127**, 054306 (2020); https://doi.org/10.1063/1.5133809

The quantum spin Hall effect and topological insulators
Physics Today **63**, 33 (2010); https://doi.org/10.1063/1.3293411

Origin of planar Hall effect in type-II Weyl semimetal MoTe$_2$
AIP Advances **9**, 055015 (2019); https://doi.org/10.1063/1.5094231

Observation of planar Hall effect in topological insulator—Bi₂Te₃

Archit **Bhardwaj**,[1] Syam Prasad P.,[2] Karthik V. Raman,[1,a] (iD) and Dhavala Suri[1,a] (iD)

AFFILIATIONS

[1]Tata Institute of Fundamental Research, Hyderabad, Telangana 500046, India
[2]Indian Institute of Technology Hyderabad, Sangareddy, Telangana 502285, India

[a]Authors to whom correspondence should be addressed: kvraman@tifrh.res.in and dhavalas@tifrh.res.in

ABSTRACT

Planar Hall effect (PHE) in topological insulators (TIs) is discussed as an effect that stems mostly from conduction due to topologically protected surface states. Although surface states play a critical role and are of utmost importance in TIs, our present study in Bi₂Te₃ thin films reflects the need for considering the bulk conduction in understanding the origin of PHE in TIs. This necessity emerges from our observation of an unconventional increase in the PHE signal with TI thickness and temperature where the bulk effect takes over. Here, we find an enhancement in the PHE amplitude by doubling the Bi₂Te₃ film-thickness on the Si (111) substrate—from ≈ 1.9 nΩ m in 14 quintuple layer (QL) to ≈ 3.1 nΩ m in 30 QL devices at B = 5 T. Also, the PHE amplitude in the 30 QL Bi₂Te₃ films grown on two different substrates, viz., Si (111) and Al₂O₃ (0001), shows an increase with temperature. Our experiments indicate that the contribution of bulk states to PHE in TIs could be significant.

Published under an exclusive license by AIP Publishing. https://doi.org/10.1063/5.0053498

Topological insulators (TIs) have been the forerunners of research in condensed matter physics due to the plethora of possibilities that surface states offer for fundamental exploration.[1–3] However, it is worthwhile to investigate the mesoscopic transport dominated by the bulk states.[4–7] A phenomenon that has evoked widespread interest in recent times is the planar Hall effect (PHE), which is the development of transverse voltage in response to longitudinal current, under external in-plane magnetic field, in a configuration where transverse voltage due to Lorentz force is zero. The discovery of PHE dates back to 1954[8] and has been used extensively for its application to Hall sensors.[9] PHE based magnetic random access memory devices are also known for memory storage applications.[10] Hence, nonmagnetic materials exhibiting PHE are potential candidates for such applications since they eliminate spurious fringe field effects. PHE has been observed in a variety of systems such as ferromagnet/normal metal bilayers,[11,12] ferromagnetic semiconductors,[13,14] ferromagnetic metals,[15] and topological superconductors.[16,17] Recently, the effect is in the spotlight due to its role in probing topological characteristics such as chirality. In Weyl semimetals, the origin of PHE coupled with negative magnetoresistance is considered a signature of chiral anomaly.[18–24] The origin of nonzero off diagonal terms in the resistivity tensor could be attributed to several mechanisms including classical orbital magnetoresistance.[25] However, conventional PHE refers to

transverse and longitudinal resistivities under in-plane magnetic field, given by the following equations, where periodicity of PHE is π:

$$
\begin{aligned}
\rho_{xy} &= (\rho_{\parallel} - \rho_{\perp}) \sin\phi \cos\phi, \\
\rho_{xx} &= \rho_{\perp} + (\rho_{\parallel} - \rho_{\perp}) \cos^2\phi,
\end{aligned} \tag{1}
$$

where ϕ is the angle between the current and magnetic field directions lying in the same plane, ρ_{xy} and ρ_{xx} are the transverse and longitudinal resistivities, respectively, and $\rho_{\parallel}$ and $\rho_{\perp}$ are the longitudinal resistivities when ϕ is 0° and 90°, respectively.

PHE in topological insulators is believed to stem from surface state conduction. This was demonstrated by Taskin *et al.*,[26] where the PHE amplitude measured across the Fermi level exhibited local maxima on either side of the Dirac point in the surface state regime. Bulk crystals of Sn doped Bi₁.₁Sb₀.₉Te₂S[27] also exhibit an oscillating PHE, which appears only in the topologically protected surface state regime. It is interesting to note that there is no experimental report of conventional PHE in Bi₂Se₃ despite being extensively studied.[28–30] However, it does exhibit a nonlinear unconventional PHE,[31] which refers to PHE with a periodicity of 2π. Such an unconventional PHE is also observed by Rakhmilevich *et al.*,[32] in Bi₀.₂₂Sb₀.₇₈Te₃/EuS, where induced ferromagnetism shows anisotropic magnetoresistance along with the PHE of periodicity 2π. Following these experiments, several

groups have worked on explaining the results theoretically: (i) Zheng *et al.*[33] show that PHE can arise as a consequence of anisotropic back-scattering from the Dirac cone, tilted due to in-plane magnetic field. Including nonlinear terms in momentum to the surface state Hamiltonian explains the experimental result by Taskin *et al.*, without the need to invoke scattering by impurities. (ii) Further, Nandy *et al.*[34] model PHE in TIs in the bulk conduction limit using the Boltzmann transport equation and notice that PHE arises purely from the Berry curvature of bulk bands. (iii) A recent calculation[35] using scattering theory shows that PHE in surface states of a TI stems from the trans-verse displacement of the dispersions under in-plane magnetic field and extends the calculations to spin–orbit coupled systems as well.[36] We recognize that a comprehensive satisfactory understanding of PHE in topological insulators is yet to be developed. We attempt to address this and present our experimental results.

In this article, we performed PHE experiments in thin films of Bi_2Te_3 by rotating the magnetic field in-plane by an angle ϕ with respect to the direction of current. Bi_2Te_3[30,37–44] is a three-dimensional (3D) TI with a small bulk bandgap <0.15 eV (Ref. 45) owing to which it is experimentally challenging to separate the bulk and surface contributions to the transport. An in-plane magnetic field has no orbital effect on the surface of the TI but does cause a trans-verse shift in the Dirac cone. Hence, the development of a response to in-plane magnetic field is intriguing.[46,47] It is an interesting question to ask if PHE can be observed in a bulk conduction dominated 3D-TI. To answer this question, we examined the transport dynamics of Bi_2Te_3 whose relatively small bulk bandgap allows a significant mixing of the bulk and surface state signals. We investigate PHE in Bi_2Te_3 films of two different thicknesses grown on different substrates. The following sections describe the growth of the films and the results of measurements and discuss the plausible mechanism.

High quality epitaxial films of Bi_2Te_3 were deposited on Si (111) and Al_2O_3 (0001) substrates using molecular beam epitaxy technique at a base pressure of $\approx 10^{-9}$ mTorr. A constant rate ratio of 1:10 was maintained during growth of all the samples to ensure a Te rich growth atmosphere. A two-step growth process was employed. Substrate temperature was maintained at 230 °C for Al_2O_3 (0001) and 200 °C for Si (111) optimized to attain the epitaxial film for the first 4 quintuple layers (QL). The samples were then annealed at 270 °C for 30 min, and the remaining thickness of the sample was grown at 270 °C. Thicknesses of 14 quintuple layers (QL) and 30 QL were grown on both substrates. All the samples were capped with 2 nm of Te followed by 5 nm of Al_2O_3. Transport measurements were performed in a variable temperature insert cryostat coupled with the Attocube rotation stage for angle dependent scans; samples could reach a stable lowest temperature of 1.5 K. A Keithley current source (6221) and a nanovoltmeter (2182A) were used for DC resistance measurements. All the samples were manually patterned into Hall bars for measurements, thus avoiding any contamination due to litho-graphic processes. For the rest of the manuscript, we use the nomen-clature of the samples: BSi14 and BSi30 for Bi_2Te_3 on Si (111) of 14 and 30 QL, respectively, BA14 and BA30 for Bi_2Te_3 on Al_2O_3 (0001) of 14 and 30 QL, respectively.

Basic characteristics of the films were analyzed by XRD spectra [Fig. 1(a)], which show sharp characteristic Bi_2Te_3 peaks. Raman spec-tra of the films show characteristic Bi_2Te_3 phase as well (refer to the supplementary material). The resistivity vs temperature curves
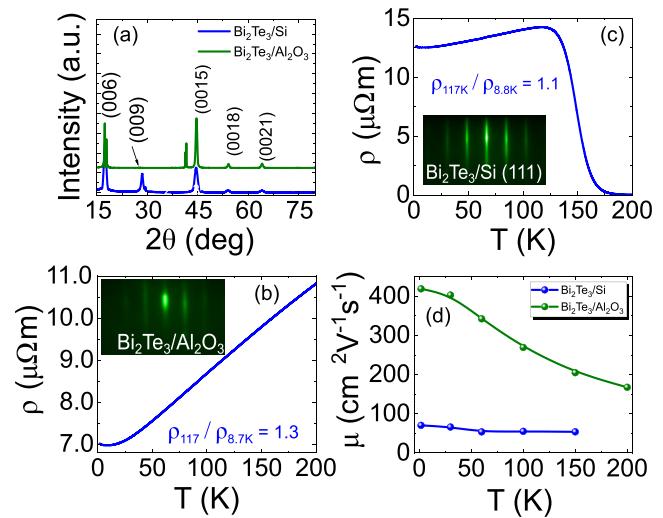

FIG. 1. (a) XRD spectrum of Bi_2Te_3 grown on Si (111) and Al_2O_3 (0001). Resistivity vs temperature and RHEED images (inset) of 14 QL Bi_2Te_3 grown on (b) Al_2O_3 (0001) and (c) Si (111). (d) Mobility vs temperature for BSi14 (blue) and BA14 (green).

[Figs. 1(b) and 1(c)] of the two films show a metallic nature. The minor upturn in resistance at low temperatures for T < 10 K may be attributed to the significant contribution from impurity bands[48,49] or the e–e interaction. RHEED images shown in the inset exhibit highly epitaxial growth. We also remark that both films show hexagonal sym-metry corresponding to the substrate indicative of epitaxial growth. Mobility calculated from the Hall measurements for BA14 is higher than that of BSi14 [Fig. 1(d)]. This may be attributed to compressive strain on the films due to lattice mismatch, which is 9% for Bi_2Te_3 grown on Al_2O_3 and 18% on Si substrates.[50,51]

The key result of our work is the demonstration of the planar Hall effect in Bi_2Te_3 and its uncommon response to temperature and film-thickness. We measure the transverse resistivity as a function of ϕ [inset of Fig. 2(a)]. ρ_{xy} varies as $\sin 2\phi$ with a period of π [Fig. 2(a)], as expected for the case of conventional PHE. We observe that the PHE amplitude (ρ_{xy} at $\phi = 45°$) varies monotonically with field and fits to the B^2 functional form [inset of Figs. 2(b) and 2(c)]. The longitu-dinal magnetoresistance (ρ_{xx}) varies as $\cos^2\phi$ consistent with Eq. (1) for conventional PHE (refer to the supplementary material). The PHE amplitude monotonically decreases with an increase in temperature [Fig. 2(d)], indicating that either (i) surface state contribution to the PHE signal is decreasing with temperature or (ii) bulk disorder-induced thermal excitations decrease the PHE signal from the bulk states of BA14 and BSi14 devices [refer to the supplementary material PHE amplitude vs T of Bi_2Te_3/Si (111)]. In the low mobility BSi14, either or both of the above effects may dominate causing a decrease in PHE amplitude with temperature. However, in the case of BA14 devi-ces having six times higher mobility than in BSi14, the contribution of the latter effect may be less, suggesting a more dominant surface con-tribution to the total PHE amplitude. This may also explain the larger magnitude of the PHE amplitude in BA14 compared to that of BSi14. Experiments by Taskin *et al.*[26] and Wu *et al.*[27] have demonstrated that PHE dominated by surface states decays with temperature in
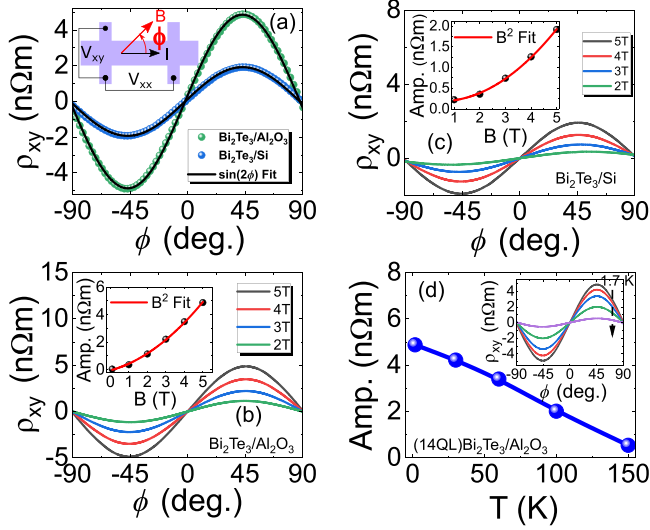
FIG. 2. (a) ρ_{xy} vs azimuthal angle (ϕ) for BSi14 (blue) and BA14 (green) with $\sin 2\phi$ fit (black line) at $B = 5$ T; the inset shows the schematic of measurement geometry. ρ_{xy} vs ϕ at different in-plane magnetic fields for (b) BA14 and (c) BSi14; the insets show B^2 fit. (d) PHE amplitude ($\rho_{xy}(\phi = 45°)$) for BA14 at $B = 5$ T. The inset shows the corresponding ρ_{xy} vs ϕ.
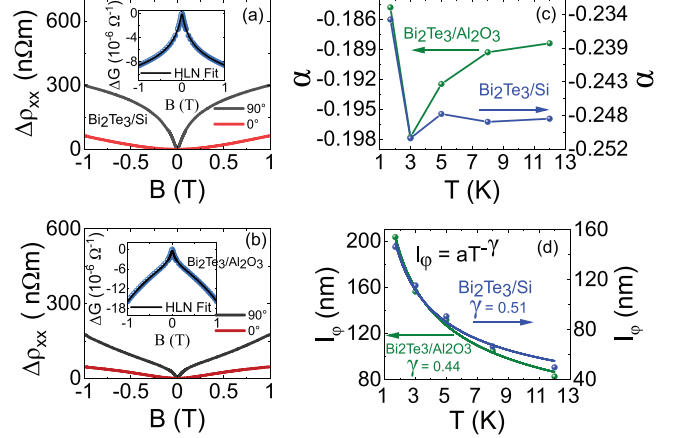

FIG. 3. ρ_{xx} vs B at out-of-plane and in-plane magnetic fields for (a) BSi14 and (b) BA14. The insets show magnetoconductance with HLN fit. HLN parameters extracted from out-of-plane magnetotransport measurement (inset) for both devices (c) prefactor (α) vs temperature (d) coherence length (l_φ) vs temperature. $\Delta\rho_{xx} = \rho(B) - \rho(0)$.

$Bi_{2-x}Sb_xTe_3$ and $Bi_{1.1}Sb_{0.9}Te_2S$, respectively. Alternatively, the difference in PHE amplitude of the two devices can be explained from the chemical potential arguments. The chemical potential in BA14 is lower than that in BSi14,[26] suggesting a larger surface contribution calculated using free-electron approximation ($m^* = 0.1\, m_e$, where $m_e = 9.1 \times 10^{-31}$ kg and m^* is the effective mass) to be lying 0.34 and 0.58 eV above the conduction band edge for BA14 and BSi14 devices, respectively. We remark that this is only a crude approximation since it does not consider the precise dispersion relation for each sample.

It is fruitful to study the magnetotransport in the out-of-plane magnetic field direction to understand the interplay of scattering from scalar impurities and spin–orbit coupling.[52] As shown in Figs. 3(a) and 3(b), the resistivity of the sample shows a cusp at low field when the sample is perpendicular to the plane of magnetic field, indicating weak antilocalization (WAL). By rotating the sample from out-of-plane to in-plane magnetic field configuration (θ is rotated from 90° to 0°), we find that the cusp vanishes and resistivity decreases. The magnetoconductance cusp (insets of Fig. 3(a) and (b)) is fit to the Hikami–Larkin–Nagaosa (HLN) model [Eq. (2)][53] that best explains the scattering and quantifies the coherence length (l_φ) and α whose values indicate the number of conducting 2D channels in the transport and the mechanism responsible for dephasing, respectively,

$$\Delta G = \sigma(H) - \sigma(0) = -\alpha \frac{e^2}{\pi h}\left\{\Psi\left(\frac{1}{2} + \frac{B_\phi}{H}\right) - \log\left(\frac{B_\phi}{H}\right)\right\}, \quad (2)$$

where $B_\phi = \frac{h}{8\pi e l_\varphi^2}$ and Ψ is the digamma function (refer to the supplementary material for details on fitting routine). The coherence length l_φ at 1.7 K is ≈ 160 and 200 nm for BSi14 and BA14, respectively [Fig. 3(d)]. The power law $l_\varphi = aT^\gamma$ fit to the temperature dependence of l_φ shows that the dephasing mechanism is likely to be e–e interaction.[54] α [Fig. 3(c)] is ≈ 0.19 and 0.23 for BA14 and BSi14,

respectively. In the ideal case, the value of α is expected to be 1/2 for conduction due to single coherent channel. However, the observed lower values of α indicate that the bulk conduction dominates the transport in our Bi_2Te_3 samples irrespective of the substrate. WAL signal decays for $T > 10$ K; however, the PHE persists up to much higher temperatures, implying that the origin of the two effects is uncorrelated. For a comprehensive picture of the various parameters of the Bi_2Te_3 devices discussed in the manuscript, we illustrate the comparison in Table I.

Since it is important to understand if the origin of PHE stems from the surface or the bulk, we examine PHE in thicker samples (thickness = 30 QL) of Bi_2Te_3 maintaining exactly the same growth conditions as the respective thinner samples. Figure 4(a) shows the transverse resistivity as a function of magnetic field, which exhibits a conventional behavior: PHE amplitude varies as B^2 and is sinusoidal with respect to ϕ. We compare the relative PHE amplitudes of the thicker and thinner film devices [Fig. 4(b)]. It is intriguing that the PHE amplitude of the BSi30 sample is higher than that of the BSi14 at $B = 5$ T. However, the magnitude of the PHE amplitude in BA30 drops relative to that of BA14 [Fig. 4(d)]. Relative to the respective thinner samples, the mobility in BSi30 enhances ≈ 6 times as

TABLE I. Summary of structural and transport properties of Bi_2Te_3 samples discussed in the manuscript.

Thickness	14 QL		30 QL	
Substrate	Al_2O_3	Si	Al_2O_3	Si
Mobility ($cm^2\,V^{-1}\,s^{-1}$)	401	70	670	418
Carrier conc. ($\times 10^{19}\,cm^{-3}$)	2.38	7.5	1.6	2.95
Lattice constant (a = b) (Å)	4.37	4.35	4.34	4.39
α	−0.19	−0.23	−0.24	−0.24
l_φ (nm)	213	149	108	156

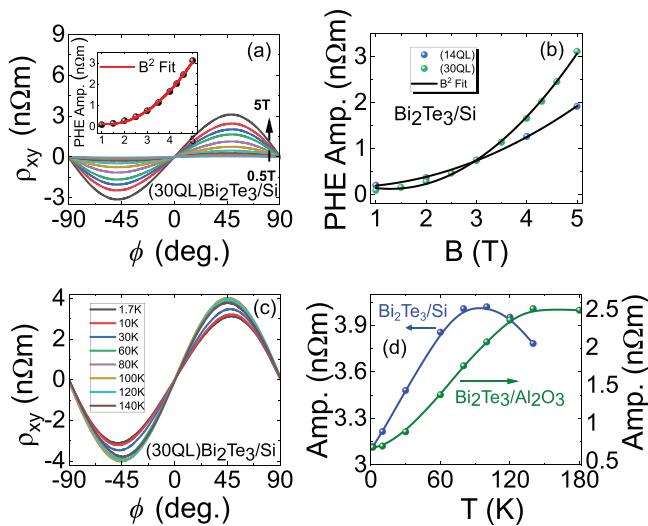**FIG. 4.** (a) ρ_{xy} vs ϕ for BSi30; the inset shows PHE amplitude vs field with B^2 fit. (b) PHE amplitude vs B for BSi14 (blue) and BSi30 (green) with B^2 fit (black). (c) ρ_{xy} vs ϕ for BSi30 at different temperatures. (d) PHE amplitude vs temperature for BSi30 and BA30. The down-turn in the PHE amplitude in BSi30 at T > 100 K appears due to increasing conduction in Si at higher temperatures.

compared to a marginal enhancement (≈ 1.7 times) in BA30; carrier concentrations of the samples do not vary significantly (refer Table I). This suggests that bulk-disorder is the primary reason for the above contrasting trends in the magnitude of PHE amplitude for the two sets of samples (BA14-BA30 and BSi14-BSi30). In BSi30, with a considerable drop in bulk-disorder, the PHE signal increases due to larger bulk contribution. While in BA30, an increase in thickness primarily reduces the surface contribution to the overall PHE amplitude explaining the drop in PHE amplitude relative to BA14. However, interestingly in both BSi30 and BA30, we observe an increase in PHE amplitude with an increase in temperature [Figs. 4(c) and 4(d)]. This contrasting trend of PHE amplitude with temperature for thicker films compared to that for the thinner films corroborates our inference that here in thicker films bulk states predominantly contribute to the PHE signal.

We now discuss all plausible mechanisms that lead to PHE in Bi_2Te_3. Taskin et al.[26] propose anisotropic lifting of topological protection of the surface states causing PHE. However, in our case, it is evident that the carrier concentrations of the samples do not correspond to the energy of the topologically protected surface state regime, where this theory could be applied. The picture of chiral anomaly is ruled out since chirality is not a well defined quantity in 3D topological insulators. Nandy et al.[34] show that a 3D-TI with negative magnetoresistance can exhibit PHE without the need to invoke chiral anomaly. This occurs purely because of the Berry curvature induced anomalous magnetotransport in the bulk limit. In our samples, correlation between weak antilocalization and planar Hall effect seems to be less since WAL exists only at low temperatures, whereas PHE persists up to relatively much higher temperatures. Zheng et al.[33] propose the existence of planar Hall voltage arising due to nonlinear terms in momentum due to spin–orbit coupling in the TI. By this theory, the emergence of PHE in 3D-TI seems to be of nontopological origin and

arises purely due to the tilt of the Dirac cone in the presence of an in-plane magnetic field. From our experiments, it is clear that PHE arises despite not being in the surface state regime of the band structure. We do not rule out the possibility that PHE is sensitive to the Fermi level position; however, this requires a rigorous calculation of the PHE specific to the band structure of Bi_2Te_3. We believe that the PHE in Bi_2Te_3 stems from the dominant bulk contribution, as evident from the observation of an increase in PHE signal with temperature in our thicker devices. While disentangling the bulk and the surface states has always been a challenge experimentally, emergence of PHE in bulk dominated TI establishes that the effect does not necessarily require surface state transport. This calls for a theoretical calculation that addresses PHE specific to the band structure of Bi_2Te_3. Our experiments pave the way for further theoretical investigation of anisotropies leading to PHE in TIs.

In conclusion, our experiment demonstrates a comprehensive study of PHE in 3D-TI Bi_2Te_3. The PHE amplitude varies as a square of the magnetic field and agrees well with the conventional PHE equations. Interestingly, the PHE amplitude enhances in BSi30 as compared to that in the BSi14. Furthermore, in contrast to the 14 QL samples, the PHE amplitude in the 30 QL samples increases with temperature. While the origin of PHE in TIs is attributed to arise because of topologically protected surface states, our experiment provides a different perspective. We infer that the PHE has a significant contribution from bulk conduction as well, paving the way for further theoretical modeling of PHE in TIs that may assist in the future development of quantum technologies.

See the supplementary material that contains data of additional devices, fitting routine, and description of calculations used in the manuscript.

DATA AVAILABILITY

The data that support the findings of this study are available from the corresponding authors upon request.

REFERENCES

[1]Y. Ando, "Topological insulator materials," J. Phys. Soc. Jpn. **82**, 102001 (2013).
[2]X.-L. Qi and S.-C. Zhang, "Topological insulators and superconductors," Rev. Mod. Phys. **83**, 1057–1110 (2011).
[3]M. Z. Hasan and C. L. Kane, "Colloquium: Topological insulators," Rev. Mod. Phys. **82**, 3045–3067 (2010).
[4]D. Backes, D. Huang, R. Mansell, M. Lanius, J. Kampmeier, D. Ritchie, G. Mussler, G. Gumbs, D. Grützmacher, and V. Narayan, "Disentangling surface and bulk transport in topological-insulator $p - n$ junctions," Phys. Rev. B **96**, 125125 (2017).
[5]H. Velkov, G. N. Bremm, T. Micklitz, and G. Schwiete, "Transport in topological insulators with bulk-surface coupling: Interference corrections and conductance fluctuations," Phys. Rev. B **98**, 165408 (2018).

[6]L. Barreto, L. Kühnemund, F. Edler, C. Tegenkamp, J. Mi, M. Bremholm, B. B. Iversen, C. Frydendahl, M. Bianchi, and P. Hofmann, "Surface-dominated transport on a bulk topological insulator," Nano Lett. **14**, 3755–3760 (2014).

[7]J. G. Checkelsky, Y. S. Hor, R. J. Cava, and N. P. Ong, "Bulk band gap and surface state conduction observed in voltage-tuned crystals of the topological insulator Bi_2Se_3," Phys. Rev. Lett. **106**, 196801 (2011).

[8]C. Goldberg and R. E. Davis, "New galvanomagnetic effect," Phys. Rev. **94**, 1121–1125 (1954).

[9]É. M. Épshtein, "Planar Hall effect in ferromagnets," Phys. Solid State **44**, 1327–1329 (2002).

[10]Y. Bason, L. Klein, J.-B. Yau, X. Hong, J. Hoffman, and C. H. Ahn, "Planar Hall-effect magnetic random access memory," J. Appl. Phys. **99**, 08R701 (2006).

[11]M. Jamali, Z. Zhao, M. DC, D. Zhang, H. Li, A. K. Smith, and J.-P. Wang, "Planar Hall effect based characterization of spin orbital torques in Ta/CoFeB/MgO structures," J. Appl. Phys. **119**, 133902 (2016).

[12]C. Safranski, E. A. Montoya, and I. N. Krivorotov, "Spin–orbit torque driven by a planar Hall current," Nat. Nanotechnol. **14**, 27–30 (2019).

[13]S. Lee, J.-H. Chung, X. Liu, J. K. Furdyna, and B. J. Kirby, "Ferromagnetic semiconductor GaMnAs," Mater. Today **12**, 14–21 (2009).

[14]Y. You, Y. Gong, H. Li, Z. Li, M. Zhu, J. Tang, E. Liu, Y. Yao, G. Xu, F. Xu, and W. Wang, "Angular dependence of the topological Hall effect in the uniaxial van der Waals ferromagnet Fe_3GeTe_2," Phys. Rev. B **100**, 134441 (2019).

[15]E. M. Epshtein, A. I. Krikunov, and Y. F. Ogrin, "Planar Hall effect in thin-film magnetic structures. Cobalt films on silicon substrates," in Second Moscow International Symposium on Magnetism [J. Magn. Magn. Mater. **258–259**, 80–83 (2003)].

[16]H. Huang, J. Gu, P. Ji, Q. Wang, X. Hu, Y. Qin, J. Wang, and C. Zhang, "Giant anisotropic magnetoresistance and planar Hall effect in $Sr_{0.06}Bi_2Se_3$," Appl. Phys. Lett. **113**, 222601 (2018).

[17]J. Ge, D. Ma, Y. Liu, H. Wang, Y. Li, J. Luo, T. Luo, Y. Xing, J. Yan, D. Mandrus, H. Liu, X. C. Xie, and J. Wang, "Unconventional Hall effect induced by Berry curvature," Natl. Sci. Rev. **7**, 1879–1885 (2020).

[18]A. A. Burkov, "Giant planar Hall effect in topological metals," Phys. Rev. B **96**, 041110 (2017).

[19]X. Wan, A. M. Turner, A. Vishwanath, and S. Y. Savrasov, "Topological semimetal and Fermi-arc surface states in the electronic structure of pyrochlore iridates," Phys. Rev. B **83**, 205101 (2011).

[20]Q. Li, D. E. Kharzeev, C. Zhang, Y. Huang, I. Pletikosić, A. V. Fedorov, R. D. Zhong, J. A. Schneeloch, G. D. Gu, and T. Valla, "Chiral magnetic effect in $ZrTe_5$," Nat. Phys. **12**, 550–554 (2016).

[21]J. Xiong, S. K. Kushwaha, T. Liang, J. W. Krizan, M. Hirschberger, W. Wang, R. J. Cava, and N. P. Ong, "Evidence for the chiral anomaly in the Dirac semimetal Na_3Bi," Science **350**, 413–416 (2015).

[22]M. Hirschberger, S. Kushwaha, Z. Wang, Q. Gibson, S. Liang, C. A. Belvin, B. A. Bernevig, R. J. Cava, and N. P. Ong, "The chiral anomaly and thermopower of Weyl fermions in the half-Heusler GdPtBi," Nat. Mater. **15**, 1161–1165 (2016).

[23]P. Li, C. Zhang, Y. Wen, L. Cheng, G. Nichols, D. G. Cory, G.-X. Miao, and X.-X. Zhang, "Anisotropic planar Hall effect in the type-II topological Weyl semimetal WTe_2," Phys. Rev. B **100**, 205128 (2019).

[24]S. Nandy, G. Sharma, A. Taraphder, and S. Tewari, "Chiral anomaly as the origin of the planar Hall effect in Weyl semimetals," Phys. Rev. Lett. **119**, 176804 (2017).

[25]Z. Li, T. Xiao, R. Zou, J. Li, Y. Zhang, Y. Zeng, M. Zhou, J. Zhang, and W. Wu, "Planar Hall effect in $PtSe_2$," J. Appl. Phys. **127**, 054306 (2020).

[26]A. A. Taskin, H. F. Legg, F. Yang, S. Sasaki, Y. Kanai, K. Matsumoto, A. Rosch, and Y. Ando, "Planar Hall effect from the surface of topological insulators," Nat. Commun. **8**, 1340 (2017).

[27]B. Wu, X.-C. Pan, W. Wu, F. Fei, B. Chen, Q. Liu, H. Bu, L. Cao, F. Song, and B. Wang, "Oscillating planar Hall response in bulk crystal of topological insulator Sn doped $Bi_{1.1}Sb_{0.9}Te_2S$," Appl. Phys. Lett. **113**, 011902 (2018).

[28]S. Wiedmann, A. Jost, B. Fauqué, J. van Dijk, M. J. Meijer, T. Khouri, S. Pezzini, S. Grauer, S. Schreyeck, C. Brüne, H. Buhmann, L. W. Molenkamp, and N. E. Hussey, "Anisotropic and strong negative magnetoresistance in the three-dimensional topological insulator Bi_2Se_3," Phys. Rev. B **94**, 081302 (2016).

[29]Y. Xia, D. Qian, D. Hsieh, L. Wray, A. Pal, H. Lin, A. Bansil, D. Grauer, Y. S. Hor, R. J. Cava, and M. Z. Hasan, "Observation of a large-gap topological-

insulator class with a single Dirac cone on the surface," Nat. Phys. **5**, 398–402 (2009).

[30]J. G. Analytis, R. D. McDonald, S. C. Riggs, J.-H. Chu, G. S. Boebinger, and I. R. Fisher, "Two-dimensional surface state in the quantum limit of a topological insulator," Nat. Phys. **6**, 960–964 (2010).

[31]P. He, S. S.-L. Zhang, D. Zhu, S. Shi, O. G. Heinonen, G. Vignale, and H. Yang, "Nonlinear planar Hall effect," Phys. Rev. Lett. **123**, 016801 (2019).

[32]D. Rakhmilevich, F. Wang, W. Zhao, M. H. W. Chan, J. S. Moodera, C. Liu, and C.-Z. Chang, "Unconventional planar Hall effect in exchange-coupled topological insulator–ferromagnetic insulator heterostructures," Phys. Rev. B **98**, 094404 (2018).

[33]S.-H. Zheng, H.-J. Duan, J.-K. Wang, J.-Y. Li, M.-X. Deng, and R.-Q. Wang, "Origin of planar Hall effect on the surface of topological insulators: Tilt of Dirac cone by an in-plane magnetic field," Phys. Rev. B **101**, 041408 (2020).

[34]S. Nandy, A. Taraphder, and S. Tewari, "Berry phase theory of planar Hall effect in topological insulators," Sci. Rep. **8**, 14983 (2018).

[35]D. Suri and A. Soori, "Finite transverse conductance in topological insulators under an applied in-plane magnetic field," arXiv:2101.07670 (2021).

[36]A. Soori, "Finite transverse conductance and anisotropic magnetoconductance in spin orbit coupled two dimensional electron gas under an applied in-plane magnetic field," arXiv:2105.05901 (2021).

[37]Y.-Y. Li, G. Wang, X.-G. Zhu, M.-H. Liu, C. Ye, X. Chen, Y.-Y. Wang, K. He, L.-L. Wang, X.-C. Ma, H.-J. Zhang, X. Dai, Z. Fang, X.-C. Xie, Y. Liu, X.-L. Qi, J.-F. Jia, S.-C. Zhang, and Q.-K. Xue, "Intrinsic topological insulator Bi_2Te_3 thin films on Si and their thickness limit," Adv. Mater. **22**, 4002–4007 (2010).

[38]H. Zhang, C.-X. Liu, X.-L. Qi, X. Dai, Z. Fang, and S.-C. Zhang, "Topological insulators in Bi_2Se_3, Bi_2Te_3 and Sb_2Te_3 with a single Dirac cone on the surface," Nat. Phys. **5**, 438–442 (2009).

[39]M. Michiardi, I. Aguilera, M. Bianchi, V. E. de Carvalho, L. O. Ladeira, N. G. Teixeira, E. A. Soares, C. Friedrich, S. Blügel, and P. Hofmann, "Bulk band structure of Bi_2Te_3," Phys. Rev. B **90**, 075105 (2014).

[40]L. Fu, "Hexagonal warping effects in the surface states of the topological insulator Bi_2Te_3," Phys. Rev. Lett. **103**, 266801 (2009).

[41]O. Concepción, V. Pereira, A. Choa, S. Altendorf, A. Escobosa, and O. de Melo, "The growth of Bi_2Te_3 topological insulator films: Physical vapor transport vs molecular beam epitaxy," Mater. Sci. Semicond. Process. **101**, 61–66 (2019).

[42]J. Krumrain, G. Mussler, S. Borisova, T. Stoica, L. Plucinski, C. Schneider, and D. Grützmacher, "MBE growth optimization of topological insulator Bi_2Te_3 films," J. Cryst. Growth **324**, 115–118 (2011).

[43]Z. Zeng, T. A. Morgan, D. Fan, C. Li, Y. Hirono, X. Hu, Y. Zhao, J. S. Lee, J. Wang, Z. M. Wang, S. Yu, M. E. Hawkridge, M. Benamara, and G. J. Salamo, "Molecular beam epitaxial growth of Bi_2Te_3 and Sb_2Te_3 topological insulators on GaAs (111) substrates: A potential route to fabricate topological insulator p-n junction," AIP Adv. **3**, 072112 (2013).

[44]D.-X. Qu, Y. S. Hor, J. Xiong, R. J. Cava, and N. P. Ong, "Quantum oscillations and Hall anomaly of surface states in the topological insulator Bi_2Te_3," Science **329**, 821–824 (2010).

[45]M. Hada, K. Norimatsu, S. Tanaka, S. Keskin, T. Tsuruta, K. Igarashi, T. Ishikawa, Y. Kayanuma, R. J. D. Miller, K. Onda, T. Sasagawa, S.-Y. Koshihara, and K. G. Nakamura, "Bandgap modulation in photoexcited topological insulator Bi_2Te_3 via atomic displacements," J. Chem. Phys. **145**, 024504 (2016).

[46]A. A. Zyuzin, M. D. Hook, and A. A. Burkov, "Parallel magnetic field driven quantum phase transition in a thin topological insulator film," Phys. Rev. B **83**, 245428 (2011).

[47]S. S. Pershoguba and V. M. Yakovenko, "Spin-polarized tunneling current through a thin film of a topological insulator in a parallel magnetic field," Phys. Rev. B **86**, 165404 (2012).

[48]J. Xiong, Y. Luo, Y. Khoo, S. Jia, R. J. Cava, and N. P. Ong, "High-field Shubnikov–de Haas oscillations in the topological insulator Bi_2Te_2Se," Phys. Rev. B **86**, 045314 (2012).

[49]Z. Ren, A. A. Taskin, S. Sasaki, K. Segawa, and Y. Ando, "Large bulk resistivity and surface quantum oscillations in the topological insulator Bi_2Te_2Se," Phys. Rev. B **82**, 241306 (2010).

[50]S. M. Young, S. Chowdhury, E. J. Walter, E. J. Mele, C. L. Kane, and A. M. Rappe, "Theoretical investigation of the evolution of the topological phase of Bi_2Se_3 under mechanical strain," Phys. Rev. B **84**, 085106 (2011).

[51]M. Brahleka, N. Koirala, N. Bansal, and S. Oh, "Transport properties of topological insulators: Band bending, bulk metal-to-insulator transition, and weak anti-localization," Solid State Commun. **215–216**, 54–62 (2015).

[52]W. E. Liu, E. M. Hankiewicz, and D. Culcer, "Weak localization and antilocalization in topological materials with impurity spin-orbit interactions," Materials **10**, 807 (2017).

[53]S. Hikami, A. I. Larkin, and Y. Nagaoka, "Spin-orbit interaction and magnetoresistance in the two dimensional random system," Prog. Theor. Phys. **63**, 707–710 (1980).

[54]H. Liu, L. Bao, Z. Zhou, B. Che, R. Zhang, C. Bian, R. Ma, L. Wu, H. Yang, J. Li, C. Gu, C.-M. Shen, S. Du, and H.-J. Gao, "Quasi-2D transport and weak antilocalization effect in few-layered VSe_2," Nano Lett. **19**, 4551–4559 (2019).